Desalination and Water Treatment
www.deswater.com

doi: 10.5004/dwt.2017.20307

65 (2017) 67–78
February

Adaptive neuro-fuzzy model for renewable energy powered desalination plant

P. Kofinas[a,b,*], A.I. Dounis[b], Essam Sh. Mohamed[c], G. Papadakis[c]

[a]*Department of Digital Systems, University of Piraeus, Piraeus, Greece, Tel. +30 210 5381533; Fax: +30 210 5381287; email: panagiotis.kofinas@gmail.com*
[b]*Department of Automation Engineering, Piraeus University of Applied Sciences (T.E.I. of Piraeus), Egaleo-Athens, Greece*
[c]*Department of Natural Resources and Agricultural Engineering, Agricultural University of Athens, Athens, Greece*

Received 30 March 2016; Accepted 28 October 2016

ABSTRACT

In this paper, a neuro-fuzzy model for a reverse osmosis desalination plant was developed for the simulation of renewable energy powered desalination units. The development of the model is based on real data gathered by an experimental pilot desalination unit installed in the Agricultural University of Athens. The model was developed by using the adaptive neuro-fuzzy inference system for the three outputs that are the current fed into the motor of the plant, the electrical conductivity and the flow rate of the produced water. The evaluation indexes of mean absolute error, root mean square error, coefficient of determination, linear correlation coefficient, nondimensional error index and percentile variance accounted for are used in order to highlight the good performance of the whole model. The value of each index for the motor current is 0.5829, 0.9151, 94.6433, 0.9816, 0.0676 and 94.6433, respectively. The value of each index for the flow rate of the potable water is 0.2489, 0.3380, 99.9933, 1, 0.0040 and 99.9933, respectively, and the value of each index for the electrical conductivity of the potable water is 41.3427, 83.9158, 90.1276, 0.9511, 0.1545 and 90.1276, respectively. The usability of the model is demonstrated in a simple simulation of power circuits.

Keywords: Desalination plant; Adaptive neuro-fuzzy modeling; Power model; Machine learning system; ANFIS

1. Introduction

The lack of potable water in many regions of the world has led to new development in desalination processes. There are different methods for water desalinating, such as distillation, electrodialysis and reverse osmosis (RO) [1]. Desalination requires the use of energy in order to produce water. Despite the fact that there are many different types of desalination techniques, today the least energy-intensive method is RO. The desalination process is essential in remote areas where they do not have access to drinking water. The produced freshwater can be stored and used in periods when the solar irradiation is low or does not exist at all (at night). Moreover, freshwater storage has been identified to have implication on the penetration of renewable energy sources [2]. Additionally, the water storage played a crucial role in the energy management of patch and semi-patch desalination systems [3]. The need for the development of a desalination power model is essential in order to make studies for areas where there is lack of both drinking water and power (no electrical grid). Furthermore, there is a lack for models simulating RO desalination plants in variable operating condition (variable pressure and flow rate). A directly connected RO desalination unit to a photovoltaic (PV) panels without energy storage will result in an intermittent operation conditions far away from the optimum operation window of the manufacture of the membranes; however, this mode of operation is proved to be suitable for lowering the specific energy consumption and lowering the investment and water production costs [4,5]. The literature shows a variety of desalination models that have been developed. Sobana and Panda [6] developed mathematical mass transfer dynamic models of a RO desalination unit for both steady

* Corresponding author.

states and transient behaviors of the process. The results of these models were compared successfully with experimental data. Al-Shayji et al. [7] developed a model of multistage flash desalination process by using a feed forward artificial neural network (ANN) architecture trained by backpropagation algorithm with momentum and variable learning rate. The model was based on real measurements acquired during winter and summer. Jafar and Zilouchian [8] modeled three different plants of desalination. They modeled a direct seawater intake model by using radial basis function network with ten input variables and one output, the recovery of the RO. A beach well seawater intake model by using radial basis function network trained by backpropagation algorithm with nine input variables and one output, the total dissolved solid, and finally, by applying the same method, they modeled a groundwater intake with five input variables and one output, the permeate flow rate [8]. Zhani and Ben Bacha [9] developed a mathematical model for steady states based on heat and mass transfer of each component of a solar multiple condensation evaporation cycle desalination unit. Libotean et al. [1] developed a RO plant model by applying a neural network approach with backpropagation and vector regression algorithms to describe temporal variations in permeate flux and salt passage and also developed an ANN model for permeate flow and separation performances for RO desalination plant (Libotean [10]). He developed a thermodynamic model of a closed air, open water humidification–dehumidification desalination system by applying mathematical equation in order to model the plate of low-grade heat collector and the humidification–dehumidification unit [11], and Perkovic et al. [12] developed a mathematical model for systems with close integration of seawater desalination and renewable energy sources that takes individual energy flows of the system in order to study the optimal solution for supplying the demands for freshwater and electricity. Hyun-Je et al. [13] developed a simple mathematical model of RO process for seawater desalination regarding factors such as recovery ratio, permeate flux, temperature and fouling mechanism. The model can make accurate predictions without taking into account the type of the used membrane. Alasfour and Abdulrahim [14] developed a mathematical model of a multistage flash brine recirculation system that considers thermo-physical properties as a function of temperature and salinity. For details purposes, the flashing stage is divided into the components of flashing pool, distillate tray and tube bundle. In this paper, mathematical equations representing physical RO processes were not used for the development of the model, instead a neuro-fuzzy model using real system operation data was developed in order to study the quality (electrical conductivity) and the flow rate of potable water in respect to the power consumption.

The neuro-fuzzy hybrid systems integrate the advantages of fuzzy systems and neural networks, that is, all parameters can be trained like a neural network within the structure of a fuzzy logic system. ANFIS is an adaptive neuro-fuzzy inference system, which was first developed by Jang [15], and it is used to describe the overall behavior of the system under interest. ANFIS modeling is essentially a multimodal model technique where simple submodels are developed and aggregated to obtain an accurate overall model output. ANFIS approach has been applied to a wide range of areas, such as nonlinear function modeling, time series prediction [16], estimation of material properties [17–19], PV systems [20] and modeling of an electrochromic device [21]. ANFIS can be used as an alternative way of model-free approach for the modeling of a desalination unit. Therefore, the objective of this study is to develop ANFIS models for modeling of the desalination unit. These models can be used as a virtual desalination plant in achieving accurate monitoring of freshwater production substituting costly and cumbersome equipment.

In the present study, three neuro-fuzzy models, one for the drinking water flow rate, one for the current consumed by the motor and one of the electrical conductivity of the produced potable water, are developed. These three models in combination are composing the RO desalination plant. This model of the RO desalination plant is useful for simulating the desalination process and taking results about the flow rate and the quality of the water regarding the power consumption as part of any power application. The models are developed by using data sets gathered by a real desalination process.

The main contributions of this work are as follows: a model of desalination plant is developed regarding the power consumption of the plant. The model is developed by ANFIS, and no complex equations are used. The performance of the model is compared with neural networks modeling and standard linear regression using evaluation indexes such as mean absolute error (MAE), root mean square error (RMSE), coefficient of determination (R^2), linear correlation coefficient (ρ), nondimensional error index (NDEI) and percentile variance accounted for (VAF). The model is suitable for simulating power applications in order to study the production and the quality of potable water regarding power consumption.

The arrangement of this paper is as follows. In section 2.1, we review some fundamentals components of RO desalination plant. In section 2.2, we analyze the data of the desalination process. In section 2.3, the structure of the ANFIS is explained. We introduce our developed model in section 2.4. In section 2.5, the training phase is described. The testing phase is described, and the results are presented in section 2.6. In section 2.7, the model is evaluated. In section 2.8, the development of the simulation model is described. In section 3, the simulation results are presented. Finally, section 4 draws conclusions and suggestions for future work.

2. Materials and methods

2.1. Study area description

The data used for the modeling and simulation of the desalination unit were obtained from an experimental pilot desalination unit installed in the Agricultural University of Athens. Detailed description and operation of the pilot desalination unit are available from [22–24]. The unit consists of two 25–40-inch spiral wound seawater Filmtec membrane modules. The nominal total capacity (freshwater production) of the unit is 2.2 m^3/d (90 L/h). A feed water positive displacement rotary vane pump pressurizes the artificial seawater (NaCl solution 50 mS/cm), from the main mixing tank to one of the two cylinders of the Clark pump. The Clark pump is the energy recovery device and substitutes the high-pressure pump in conventional

desalination units. The high-pressure brine enters the second Clark pump cylinder and exchanges its hydraulic energy with the medium feed water pressure (13 bar). The result of these actions (exchanging high pressure of the brine with the medium pressure of the feed water) is the intensification of or increasing the feed water pressure to the required membrane pressure (around 50 bar). The rotary pump is directly connected to a permanent magnet, 24 VDC motor with nominal power of 510 W. The DC power is produced from a PV array that consists of 18 Arco Solar PV panels of total peak power of 850 Wp that is connected directly to the DC motor, without batteries, in order to minimize the specific energy consumption of the desalination unit (see Figs. 1 and 2).

2.2. Data

Parameters of the desalination unit were recorded during a period of 1 week in November. The recorded operation parameters are the freshwater flow rate, freshwater electrical conductivity, operating membrane pressure, available solar irradiance, motor current and voltage. Fig. 3 shows the produced freshwater flow rate variation with the available solar irradiation in a representative day in the 11th November in Athens, while in Fig. 4 the electrical conductivity of the produced water is shown. It is noticed that due to the direct connection of the motor to the desalination unit, the produced freshwater and the electrical conductivity are following the solar irradiation pattern. The higher the solar irradiation, the higher the freshwater production, and the higher the solar irradiation, the lower the electrical conductivity of the produced potable water. Measuring interval of the data was 5 s. However, in every 5 min interval, the mean values are recorded for 7 consecutive days in November. All measurements were performed using Campbell Scientific datalogger. Some basic descriptive statistics of the data are also presented in Table 1 in comparison with the nominal operating values of the system in the last column. It can be noticed from Table 1 that due to the low solar irradiance in November, the mean values of the operating parameter of the desalination unit are generally lower than the nominal system values. When solar irradiance reaches near the nominal level (998 W/m^2), then in this situation the maximum operating values of the system parameters (column 6 – Maximum) tend to match the nominal system operating parameters.

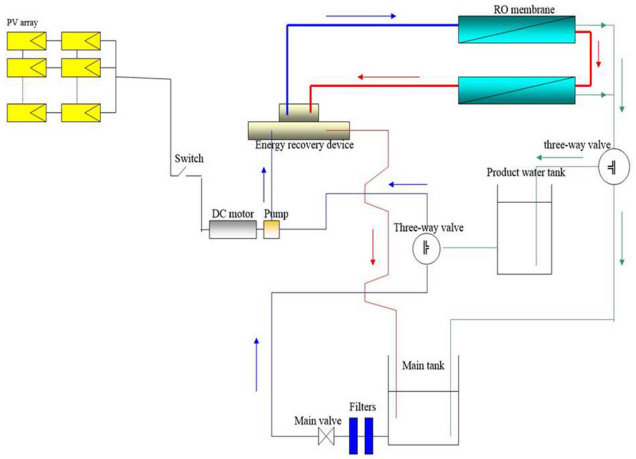

Fig. 1. Schematic diagram of the desalination unit.

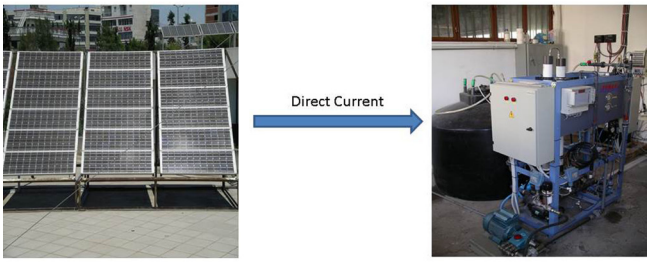

Fig. 2. Pictures from the installed (a) photovoltaic panels and (b) desalination unit.

2.3. ANFIS model description

Combining the advantages of fuzzy logic systems and neural networks:

- the local linear models (LLMs) facilitate the "minimal disturbance principle": the adaption should reduce the output error for the current training pattern, with minimal disturbance to responses already learned [25];
- the Takagi–Sugeno (T–S) fuzzy model is simple to identify because it needs less rules and parameters that can be trained from numerical data using optimization methods such as backpropagation and least-square algorithms;

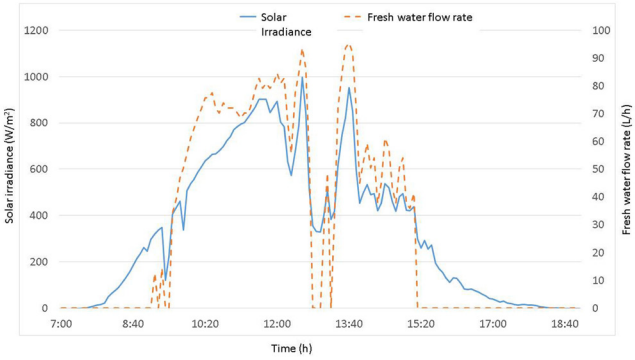

Fig. 3. Freshwater flow rate and the available solar irradiation.

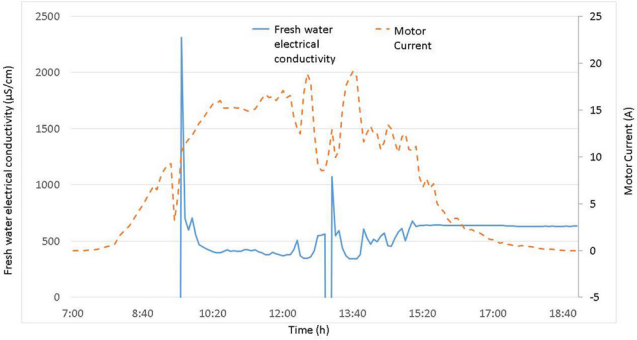

Fig. 4. Freshwater electrical conductivity and the motor current.

Table 1
Basic statistics of the experimental data

	Mean	Standard error	Median	Standard deviation	Minimum	Maximum	Confidence level (95.0%)	Nominal values
Solar irradiance (W/m^2)	372.81	26.01	343.10	298.87	0.00	998.00	51.46	1,000
Freshwater flow rate (L/h)	57.06	3.06	64.80	26.15	0.00	95.40	6.10	90
Freshwater electrical conductivity (μS/cm)	502.37	19.90	444.40	171.18	341.20	1,500.00	39.66	<1,000
Motor current (A)	9.64	0.53	10.80	5.74	0.00	19.12	1.05	20
Motor voltage (V)	12.37	0.91	14.47	9.45	0.00	28.73	1.80	24
Motor power (W)	145.53	14.12	62.09	162.19	0.00	555.06	27.93	500
Feed water pressure (bar)	6.69	0.39	7.62	3.71	0.00	12.33	0.77	12
Membrane inlet pressure (bar)	27.96	1.48	35.73	15.69	0.00	46.67	2.93	40–60

- T–S fuzzy model provides continuity of the output surface;
- T–S fuzzy models with linear rule consequent are universal approximators of any smooth nonlinear system [26]; and
- fuzzy inference system (FIS) can incorporate linguistic information as well as numerical data to achieve better performance.

ANFIS is an adaptive neuro-fuzzy inference system, which was first developed by Jang. It is a class of adaptive networks that is functionally equivalent to a first-order T–S fuzzy reasoning. The ANFIS approach learns the consequent parameters and the premise parameters of membership functions of the rules from data.

The FIS under consideration has one input x and one output y. For a first-order T–S fuzzy model [27], a general fuzzy IF-THEN rule is illustrated below:

$$R^j: \text{IF } x_1 \text{ is } A_1^j \text{ and } x_2 \text{ is } A_2^j \text{ and } \ldots x_N \text{ is } A_N^j$$

$$\text{THEN C}\hat{y}_j = a_{j1}x_1 + a_{j2}x_2 + \ldots + a_{jN}x_N + b_j$$

for $i = 1,2,\ldots, N$ and $j = 1,2,\ldots, M$, where N is the number of inputs; M is the number of rules; A_i^j is fuzzy sets; and a_{ji} and b_j are constant parameters. Fig. 5 illustrates the T–S fuzzy reasoning.

The equivalent ANFIS architecture is shown in Fig. 6. The nodes of the network in the same layer have similar functions. The ANFIS structure [15,16] consists of five layers not including input layer:

Layer 1: Every square node in this layer in ANFIS structure is adaptive node and performs fuzzification. The membership functions A_i^j are parameterized Gaussian membership functions, generalized bell function or triangular function:

$$\mu_{A_i^j}(x_i) = \exp\left[-\left(\frac{x_i - c_i^j}{\sigma_i^j}\right)^2\right] \quad (1)$$

$$\mu_{A_i^j}(x_i) = \frac{1}{1+\left[\left(\frac{x_i - c_i^j}{\sigma_i^j}\right)\right]^{b_i^j}} \quad (2)$$

$$\mu_{A_i^j}(x_i) = \begin{cases} 0, & x_i \le \rho_i^j \\ \dfrac{x_i - \rho_i^j}{m_i^j - \rho_i^j}, & \rho_i^j \le x_i \le m_i^j \\ \dfrac{k_i^j - x_i}{k_i^j - m_i^j}, & m_i^j \le x_i \le k_i^j \\ 0, & x_i \ge k_i^j \end{cases} \quad (3)$$

where A_i^j is the linguistic variables, and the set $\{\sigma_i^j, c_i^j, \rho_i^j, m_i^j, k_i^j\}$ are local adaptive parameters

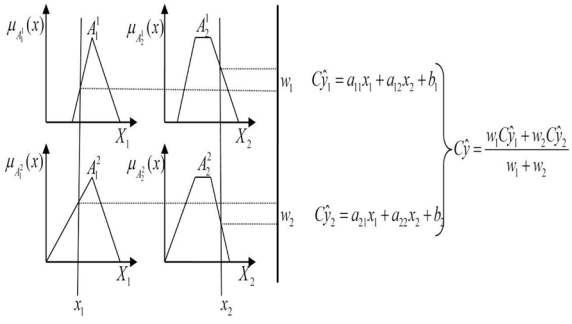

Fig. 5. A two-input first-order T–S fuzzy reasoning.

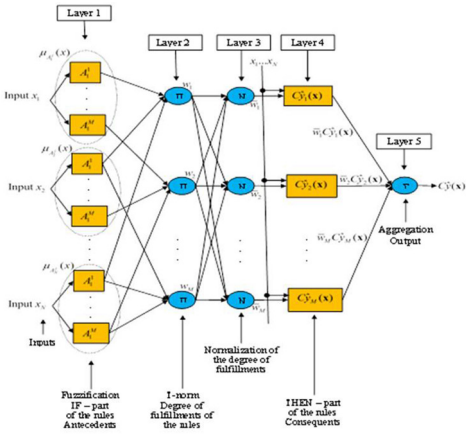

Fig. 6. Equivalent ANFIS architecture.

and known as premise parameters. Their values are updated by gradient decent during the learning phase. The node output is the fuzzy membership grade, $\mu_{A_i^j}(x_i)$.

Layer 2: This layer has so many nodes that are the fuzzy rules. Each node output represents the degree of fulfillment of a fuzzy rule. Every node can perform any T-norm operators. They are labeled Π, which perform a multiplication operator on fuzzy membership grades:

$$w_j = \prod_{i=1}^{N} \mu_{A_i^j}(x_i) \tag{4}$$

Layer 3: In the third layer, every node is fixed (circle node) and calculates the normalized of the degree of fulfillments according to the following formula:

$$\bar{w}_j = \frac{w_j}{\sum_{\lambda=1}^{M} w_\lambda} \tag{5}$$

Layer 4: The adaptive nodes in the fourth layer are the conclusive parts of fuzzy rules. Every node computes the product of the normalized degree of fulfillment and an affine function (first-order T–S model) as the following:

$$\bar{w}_j \hat{Cy}_j(x) = \bar{w}_j \left(a_{j1}x_1 + a_{j2}x_2 + \ldots + a_{jN}x_N + b_j \right) \tag{6}$$

The adaptive parameters a_{ji} and b_j in this layer will be called as consequent parameters. The liner function $\hat{Cy}(\bullet)$ is called LLM in the areas of interpolation and approximation theory.

Layer 5: Finally, in the last layer, a single fixed node labeled Σ calculates the overall network output:

$$\hat{Cy} = \sum_{j=1}^{M} \bar{w}_j \cdot \hat{Cy}_j(x) = \frac{\sum_{j=1}^{M} w_j \cdot \hat{Cy}_j(x)}{\sum_{j=1}^{M} w_j} \tag{7}$$

The fuzzy rules are actually LLMs [28]. The interpolation of these LLMs achieves global mappings, that is, identification of nonlinear relationships.

The ANFIS uses a hybrid learning procedure strategy in order to train the network. In the forward pass of the hybrid learning, the least-square method is used to optimize the consequent parameters of T–S type rules (layer 3). In the backward pass, the gradient-decent method is used to optimize the premise parameters of rules (layer 1).

The neuro-fuzzy models are developed by the toolbox "genfis2" of Matlab [29]. "Genfis2" generates a Sugeno-type FIS structure using subtractive clustering. The extraction method of the rules uses the subtractive function to determine the number of rules and antecedent membership functions and then uses linear least squares estimation to determine each rule's consequent equations. This results in an FIS structure that contains a set of fuzzy rules to cover the feature space. The type of the input function is Gaussian curve membership function 'gaussmf', and the output membership function type is 'linear'.

2.4. ANFIS desalination models

The block diagram of the desalination model can be seen in Fig. 7. The model consists of three ANFIS, the ANFIS for the electrical conductivity of the produced water, the ANFIS for the flow of the produced water and the ANFIS of the motor current. The first ANFIS (electrical conductivity) has two inputs which are the power and the electrical conductivity of the produced water in the previous state and one output which is the electrical conductivity of the water. The second one has one input which is the power and one output which is the flow of the produced water. The third one which is the motor ANFIS has one input which is the voltage across the motor and one output which is the current fed into the motor.

2.5. Training phase

1,000 measured data sets (inputs-outputs) are used for the training process of each ANFIS. Figs. 8, 10 and 12 are presenting the data sets and the centers of the clusters (red-filled circles) for each ANFIS. The method, which is used, is the subtractive clustering, and the parameters for each data set are presented in Table 2. The subtractive clustering was selected instead of the grid partition and fuzzy c-means. The developed models using grid partition did not perform adequate and similar to ones that developed with subtractive clustering. In order to achieve similar performance, a lot of rules have to be used. Additionally, in the case of the

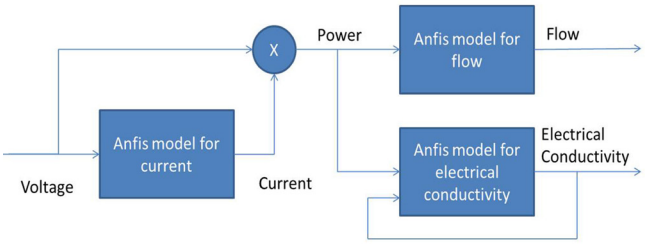

Fig. 7. Block diagram of desalination model.

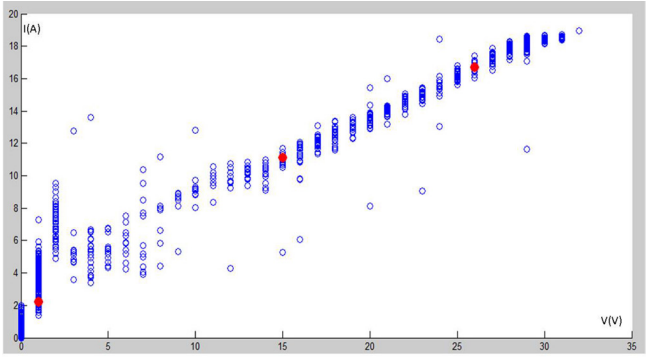

Fig. 8. Data pairs for current and voltage.

electrical conductivity where the inputs are two, the number of the rules is raising exponentially. The usage of the fuzzy c-means is recommended in more complex models where there are a lot of inputs.

The centers of the clusters are presented numerically in Table 3. For the model of the motor current, three clusters are formed while for the model of the flow rate and the electrical conductivity four and seven are formed, respectively. A data set is defined as the center of the cluster when it is surrounded by other data sets of the group. Figs. 9, 11 and 13 are showing the structure of each ANFIS model in which the amount of the nodes in the hidden layer is corresponding to the number of the clusters. The learning mechanism is the hybrid, and 2,000 epochs are applied for all the models.

Tables 4, 6, 8 and 9 present the membership functions of the inputs variables that arise after the training of the ANFIS. The Gaussian membership functions are most popular types for specifying the fuzzy set because of their smoothness, non-zero at each point and only two parameters for tuning. These parameters are the center of the peak (c) and the standard deviation (σ). Tables 5, 7 and 10 present the rule base for the output of the motor current, the flow rate and the electrical conductivity, respectively. The current of the motor consists by three first-order Sugeno type rules, the flow rate by four rules and the electrical conductivity by seven rules.

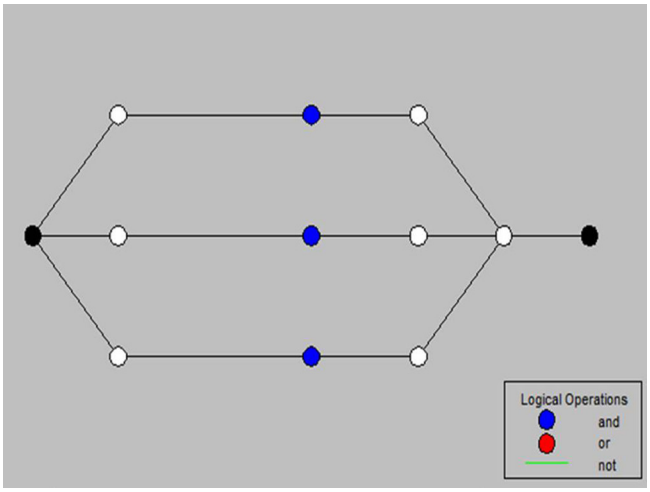

Fig. 9. Architecture of ANFIS for current.

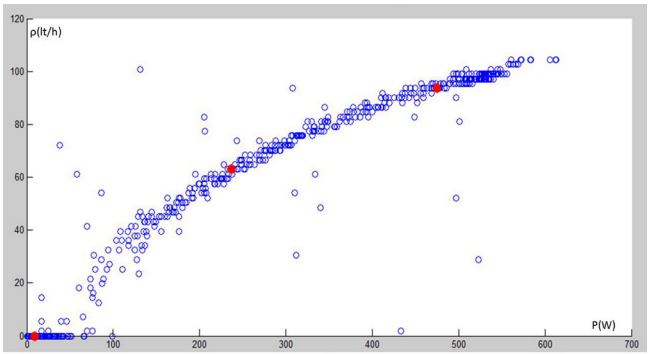

Fig. 10. Data pairs for water flow and power.

2.6. Testing phase

The data were divided into two separate sets: the training data set was used to train the ANFIS and test data to verify the accuracy and effectiveness of the trained ANFIS models. The data sets, which are used to evaluate the performance of the models, are 250. Scatterplots between the measurement data and the calculated data are presented in Figs. 14, 15 and 16. Fig. 14 presents the calculated values and the measure values of the motor current with respect to the input voltage. Additionally, it presents the fitted regression line and the best fitted line (the ANFIS model line). In most of the cases, the measured data are coincident to the calculated data with some exception in regions where one input value has many different measured values. Fig. 15 presents the calculated values and the measured values of the flow rate of the potable water with respect to the input power. It also presents the line of the ANFIS model and the line arising by the regression. The real values and the calculated values are almost coincident in any region. Fig. 16 presents the calculated values and the measure values of the electrical conductivity of the potable water with respect to the inputs of the power and the electrical conductivity of the water in the previous state. In this case, the measured values and the calculated values are not coincident in most of the cases but are very near.

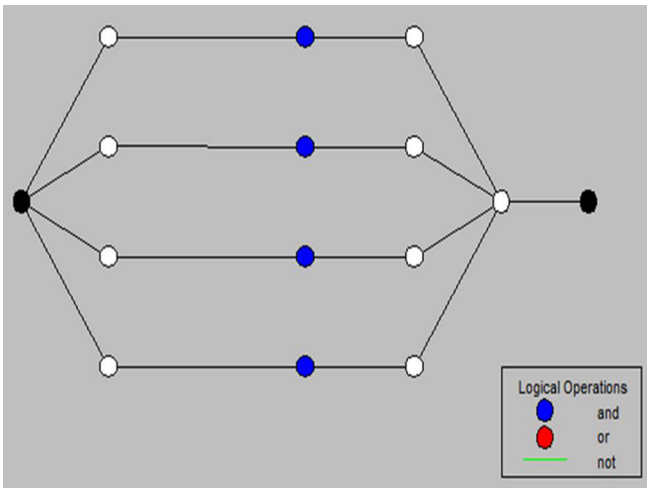

Fig. 11. Architecture of ANFIS for water flow.

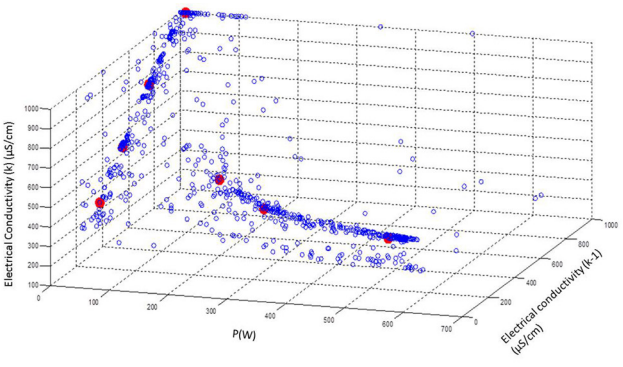

Fig. 12. Data pairs for electrical conductivity, power and electrical conductivity in the previous state.

Table 2
Parameters of subtractive clustering

ANFIS Parameters	Current	Flow	Electrical conductivity
Range of influence	0.5	0.5	0.3
Squash factor	1.25	1.25	1.25
Accept ratio	0.5	0.5	0.1
Reject ratio	0.15	0.15	0.05

Table 3
Centers of data clusters

Electrical conductivity	Flow	Current
(9, 1,000, 1,000)	(7, 0)	(1, 2.24)
(507, 304.3, 305.1)	(508, 97.2)	(26, 16.7)
(0, 754, 754)	(283, 70.2)	(15, 11.1)
(4, 536.2, 543.7)	(164, 46.8)	–
(281, 368.5, 371.39)	–	–
(10, 327.6, 364.6)	–	–
(185, 461.8, 453.2)	–	–

Table 4
Input parameters of voltage for current neuro-fuzzy model

Input	Type of MF	Linguistic values	MF parameters	
			σ	*c*
V	Gaussian	Small	10.3	–1.9
	Gaussian	Medium	7.9	10.1
	Gaussian	Big	6.9	21.0

Table 5
Rule base for the model of current

Number	Rules
1	IF V is small, THEN $I_1 = 17V + 87.8$
2	IF V is medium, THEN $I_2 = 1.4V - 37$
3	IF V is big, THEN $I_3 = 8.2V - 192.8$

Table 6
Input parameters of power for the neuro-fuzzy model of flow

Input	Type of MF	Linguistic values	MF parameters	
			σ	*c*
P	Gaussian	Zero	60.8	0.5
	Gaussian	Small	63.5	147.5
	Gaussian	Medium	62.9	267.8
	Gaussian	Big	65.7	507.6

2.7. Model performance indices

For each network, the results were graphed, and error analysis was carried out to monitor the accuracy of modeling.

Table 7
Rule base for the neuro-fuzzy model of flow

Number	Rules
1	IF P is zero, THEN $p_1 = 0.08P + 34.3$
2	IF P is small, THEN $p_2 = 0.12P + 39.8$
3	IF P is medium, THEN $p_3 = 0.1P + 47.7$
4	IF P is big, THEN $p_4 = -0.08P - 2.4$

Table 8
Input parameters of power for electrical conductivity neuro-fuzzy model

Input	Type of MF	Linguistic values	MF parameters	
			σ	*c*
P	Gaussian	Zero	64.6	1.8
	Gaussian	Very small	62.3	7.7
	Gaussian	Small	67.4	8.2
	Gaussian	Medium	64.4	10.9
	Gaussian	Big	64.7	185
	Gaussian	Very big	64.9	280.8
	Gaussian	Very very big	65	507.1

Table 9
Input parameters of previous state electrical conductivity for electrical conductivity neuro-fuzzy model

Input	Type of MF	Linguistic values	MF parameters	
			σ	*c*
$C(k-1)$	Gaussian	Zero	86.6	304.6
	Gaussian	Very small	85.1	327.6
	Gaussian	Small	84.3	368.2
	Gaussian	Medium	85.3	461.9
	Gaussian	Big	85.2	543.6
	Gaussian	Very big	85.3	765.1
	Gaussian	Very very big	85.2	1,000

Table 10
Rule base for the neuro-fuzzy model of electrical conductivity

Number	Rules
1	IF P is very small and $C(k-1)$ is very very big, THEN: $C_1 = -2P + 1\ C(k-1) - 8$
2	IF P is very very big and $C(k–1)$ is zero, THEN: $C_2 = -0.1P + 0\ C(k-1) + 356.9$
3	IF P is medium and $C(k–1)$ is very big, THEN: $C_3 = -0.2P + 1.1\ C(k-1) + 45.9$
4	IF P is zero and $C(k-1)$ is big, THEN: $C_4 = 2.8P + 1.1\ C(k-1) - 74.3$
5	IF P is very big and $C(k-1)$ is small, THEN: $C_5 = 0.1P + 0.8\ C(k-1) + 20.5$
6	IF P is small and $C(k-1)$ is very small, THEN: $C_6 = 0.9P + 0.5\ C(k-1) + 273$
7	IF P is big and $C(k-1)$ is medium, THEN: $C_7 = -0.2P + 0.1\ C(k-1) + 395.5$

Additionally, in order to highlight the performance of the ANFIS models, they are compared with models arised by multiple linear regression (MLR) and ANNs. The ANNs, which are used, are feed forward backpropagation networks with one hidden layer and sigmoid transfer function in the nodes. For the training, the method of the gradient descent is used with 2,000 iterations and a learning rate of η = 0.01. For the model of the current motor, the hidden layer consists of three neurons; for the model of the flow rate, the hidden layer is composed of four neurons; and for the model of the electrical conductivity, seven neurons are used. The performance of the ANFIS model is gauged according to the criteria: MAE, RMSE, R^2, ρ, NDEI [28], which is defined as the RMSE divided by the standard deviation of the target series, and the VAF, as follows:

$$\mathrm{MAE} = \frac{1}{N}\sum_{k=1}^{N}\left|y(k) - \hat{y}(k)\right| \tag{8}$$

$$\mathrm{RMSE} = \sqrt{\frac{1}{n}\sum_{k=1}^{n}(y(k) - \hat{y}(k))^2} \tag{9}$$

$$R^2 = \frac{\sum_{k=1}^{N}\left(\hat{y}(k) - \bar{y}\right)^2}{\sum_{k=1}^{N}\left(y(k) - \bar{y}\right)^2} \cdot 100\% \tag{10}$$

$$\rho = \frac{\sum_{k=1}^{N}(y(k) - \bar{y}) \cdot (\hat{y}(k) - \bar{\hat{y}})}{\sqrt{\sum_{k=1}^{N}(y(k) - \bar{y})^2 \cdot \sum_{k=1}^{N}(\hat{y}(k) - \bar{\hat{y}})^2}} \tag{11}$$

$$\mathrm{NDEI} = \frac{\mathrm{RMSE}}{\mathrm{std}(y)} == \sqrt{\frac{\sum_{k=1}^{n}(y(k) - \hat{y}(k))^2}{\sum_{k=1}^{n}(y(k) - \bar{y}(k))^2}} \tag{12}$$

$$\mathrm{VAF} = \left(1 - \frac{\mathrm{var}\left(y(k) - \hat{y}(k)\right)}{\mathrm{var}\left(y(k)\right)}\right) \cdot 100\% = \left(1 - \frac{\sum_{k=1}^{N}\left(e(k) - \bar{e}\right)^2}{\sum_{k=1}^{N}\left(y(k) - \bar{y}\right)^2}\right) \cdot 100\% \tag{13}$$

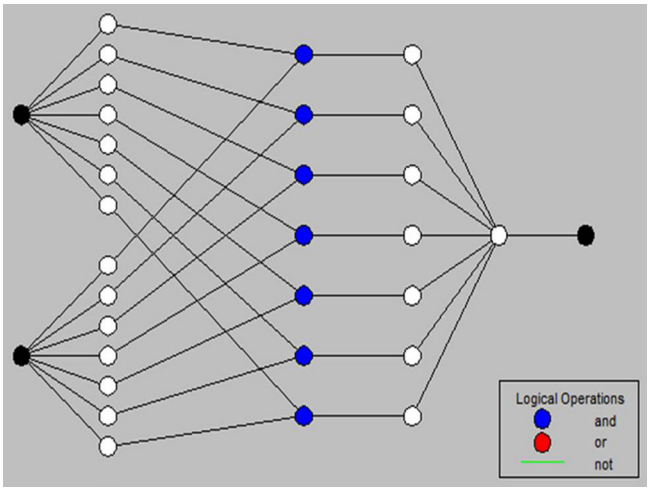

Fig. 13. Architecture of ANFIS for electrical conductivity.

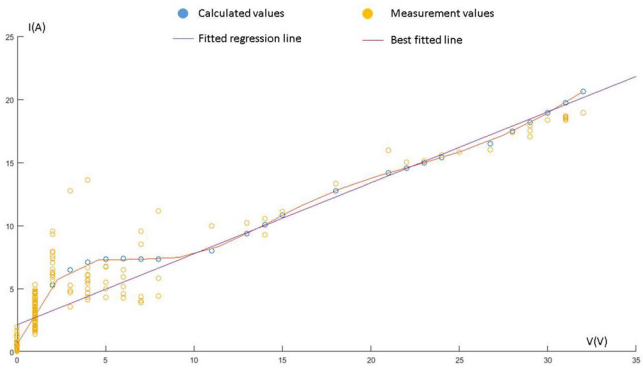

Fig. 14. Scatterplot between measurement and calculated data for ANFIS of current motor.

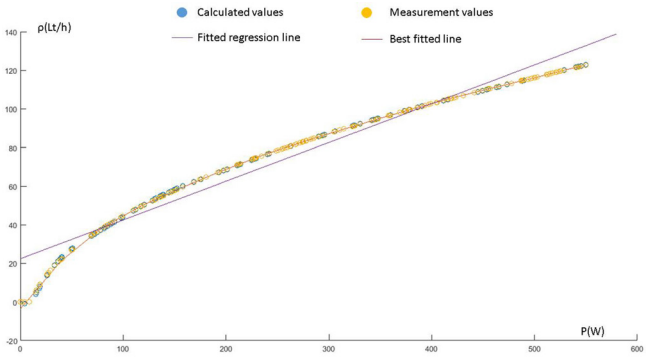

Fig. 15. Scatterplot between measurement and calculated data for ANFIS of water flow rate.

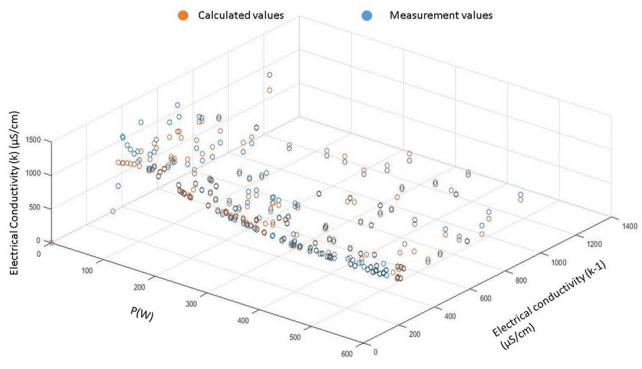

Fig. 16. Scatterplot between measurement and calculated data for ANFIS of water electrical conductivity.

$$\text{where } \operatorname{var}(y) = \text{variance(y)} = \frac{1}{N}\sum_{k=1}^{N}\left(y(k)-\bar{y}\right)^2,$$

$$\bar{y}(k) = \frac{1}{N}\sum_{k=1}^{N} y(k),\ e(k) = y(k) - \hat{y}(k)$$

$$\text{and } std(y) = \sqrt{\text{var}(y)}$$

The $y(k)$ is the actual value for time k; $\hat{y}(k)$ is the predicted value (model output) for the time k; n is the number of test data used for prediction; and $\bar{y}$ and $\bar{\hat{y}}$ are the mean of actual and predicted values, respectively. The first criterion measures the average error for all points. Correlation coefficient ρ (Pearson's formula) measures how well the predicted values correlate with the actual values. Clearly, correlation coefficient value closer to positive unity means better prediction. Tables 11,12 and 13 present the performance indices for the models of the motor current, the water flow rate and the water electrical conductivity compared with the models arised by MLR and ANN, respectively.

The performance indices VAF, RMSE, MAE and NDEI indicate that assessed results were highly correlated and precise whereas correlation coefficient was also within the acceptable limit. The model of the electrical conductivity seems to have lower performance but these values of the indexes are justified by taking into consideration the range of the data sets for this model (between 200 and 1,000 μS/cm).

2.8. Model of the whole desalination process

As mentioned before, the model of the desalination plant is a power model (outputs the water quality and the water flow taking into account the power consumption), which can also be used as part of a large power management system. In order to connect the desalination unit with other units of the system, the model must be able to connect to power elements. The connection of the model is achieved by using a resistance and a controlled current source (Fig. 17). The voltage across the resistance is measured. The voltage is the input to the neuro-fuzzy model, and the output of the model drives the current source. The product of the input voltage and the output current gives the amount of power that consumes the desalination unit. Fig. 18 shows the block diagram of the model for water flow and water electrical conductivity. The inputs of the models are the electrical conductivity at the previous state and the power consumed by the desalination process. At the output of the electrical conductivity, there is a variable that states the initial value of conductivity of the freshwater. Also, there is a conditional switch that keeps the value of the electrical conductivity

Table 11
Evaluation indexes for current motor model

Indexes	Value for current (ANFIS)	Value for current (MLR)	Value for current (ANN)
MAE	0.5829	0.7580	0.8180
RMSE	0.9151	1.4068	1.1570
R^2	94.6433	87.3415	91.4376
ρ	0.9816	0.9783	0.9729
NDEI	0.0676	0.1038	0.0854
VAF	94.6433	87.3415	91.4376

Table 12
Evaluation indexes for flow rate model

Indexes	Value for flow (ANFIS)	Value for flow (MLR)	Value for flow (ANN)
MAE	0.2489	1.4710	10.4274
RMSE	0.3380	1.9518	11.8990
R^2	99.9933	86.9130	86.2959
ρ	1.0000	0.9327	0.9765
NDEI	0.0040	0.2621	0.1404
VAF	99.9933	86.9130	86.2959

Table 13
Evaluation indexes for electrical conductivity model

Indexes	Value for electrical conductivity (ANFIS)	Value for electrical conductivity (MLR)	Value for electrical conductivity (ANN)
MAE	41.3427	81.0066	66.3539
RMSE	83.9158	112.4972	108.6168
R^2	90.1276	82.2573	72.2102
ρ	0.9511	0.9100	0.8770
NDEI	0.1545	0.2071	0.1994
VAF	90.1276	82.2573	72.2102

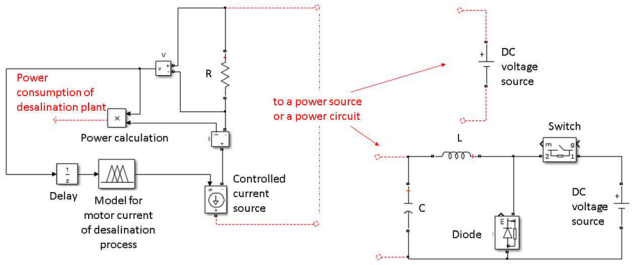

Fig. 17. Connection of desalination plant to electrical circuit.

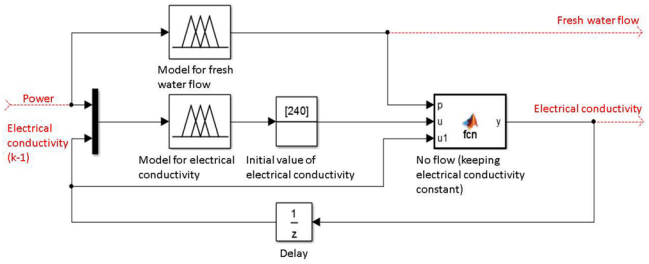

Fig. 18. Block diagram of flow and electrical conductivity of water.

constant when there is no flow. This happens because when there is no water flow, the conductivity meter continues to record the constant value of the water electrical conductivity inside. This has as a result the electrical conductivity of the water to remain unchanged. The block diagram of the whole desalination plant developed in Matlab/Simulink can be seen in Fig. 19.

3. Simulation results and discussion

The developed model is a power model that intends to be used in power applications. The model is designed to take as input voltage and by the power consumption to extract results for the flow rate and the quality of the potable water. The desalination plant model is used in a simulation of power electronics application in order to highlight the usability of the model as part of a greater power system and the operation of the plant under variable load conditions. The block diagram of the whole system is depicted in Fig. 20. It consists of a PV source, a power bank and the desalination model. A maximum power point tracking controller is used for the maximum power extraction of the source. A voltage regulator is used in order to regulate the voltage of the desalination process, and a bidirectional converter is used for the power management between the power bank, the PV source and the desalination process [30].

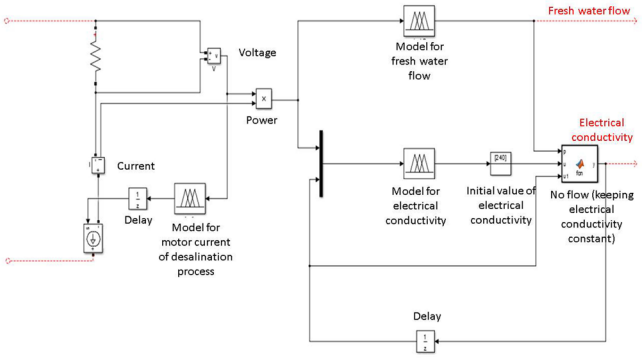

Fig. 19. Block diagram of the whole desalination process.

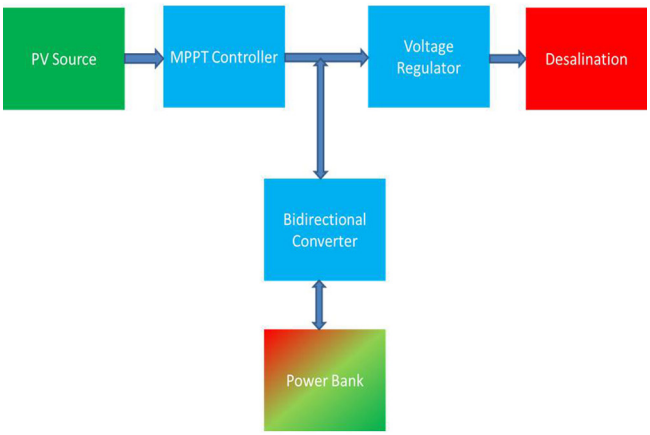

Fig. 20. Block diagram of power system.

The generated current I_{pv} of the PV model is described as:

$$I_{pv} = I_{sc} - ae^{bV_{pv}} \tag{14}$$

where:

$$I_{sc} = I_{scr}\frac{G_{pv}}{G_r}(1 + n_{iscT}(T_{pv} - T_r)) \tag{15}$$

$$a = I_{scr}e^{-b_{STC}V_{oc}} \tag{16}$$

$$b = \frac{b_{STC}}{1 + n_{vocT}(T_{pv} - T_r)} \tag{17}$$

$$b_{STC} = \frac{\log(1 - \frac{I_{mppr}}{I_{scr}})}{V_{mppr} - V_{ocr}} \tag{18}$$

where V_{pv} is the voltage across the equivalent circuit; G_r is the reference solar irradiance at standard test conditions (STC) and equals to 1,000 W/m^2; T_r is the reference temperature at STC and equals to 25°C; I_{scr} is the short circuit current of the PV source at STC; G_{pv} is the solar irradiance that incidents on the PV source; T_{pv} is the temperature of the PV source; V_{ocr} is the voltage across the PV source at STC; V_{mppr} is the voltage of the PV source at the MPP at STC; I_{mppr} is the current of the PV source at the MPP at STC; N_{vocT} is the temperature coefficient of the open circuit voltage; and n_{iscT} is temperature coefficient of the short circuit current. The characteristics of the PV source are presented in Table 14.

Figs. 21 and 22 present two different scenarios. In the first scenario (Fig. 21), the set point of the consumed power of the desalination plant remains the same while the solar irradiance is gradually rising per 100 W/m^2 from 700 W/m^2 to 1,000 W/m^2. Fig. 21(b) shows the power generated by the PV source, the power which is saved into the power bank and the power consumed to the desalination plant. While the solar irradiance raises, both the total power produced by the PV source and the power which is saving into the power bank are increased. The consumed power of the desalination plant remains the same, only a small amplitude oscillation appears after the change of the solar irradiance and for a small-time step until the system comes to equilibrium. This amplitude oscillation has as a result the flow of the produced water and the electrical conductivity to oscillate for a short period of time, until the consumed power to stabilize at the desirable level again (set point).

In the second scenario (Fig. 22), the solar irradiance remains the same while the set point of the consumed power of the desalination plant is gradually rising per 100 W from 200 W to 500 W. Fig. 22(b) shows how the power generated by the PV source remains the same while the power which is saving into the power bank is reduced when the power consumed to the desalination plant is rising. Fig. 22(c) presents the power flow and the electrical conductivity of the water. As the desalination process consumes low power (200 W),

Table 14
Characteristics of the PV source

Parameters	Description	Values
V_{ocr} (V)	The open circuit voltage of the PV source at STC	150
I_{scr} (A)	The short circuit current of the PV source at STC	8
V_{mppr} (V)	The voltage of the PV source at the maximum power point at STC	120
I_{mppr} (W)	The current that the PV source produces at the maximum power point at STC	7
n_{iscT}	Temperature coefficient of the short circuit current	0.00067
n_{vocT}	Temperature coefficient of the open circuit voltage	–0.0035

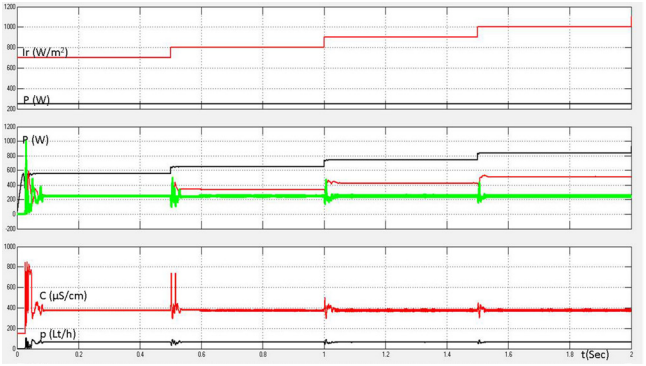

Fig. 21. (a) Solar irradiance and set point of the consumed power by the desalination plant, (b) power generated by the PV source (black), power consumed by the desalination plant (green) and power saving in the power bank (red), and (c) water electrical conductivity (red) and water flow (black).

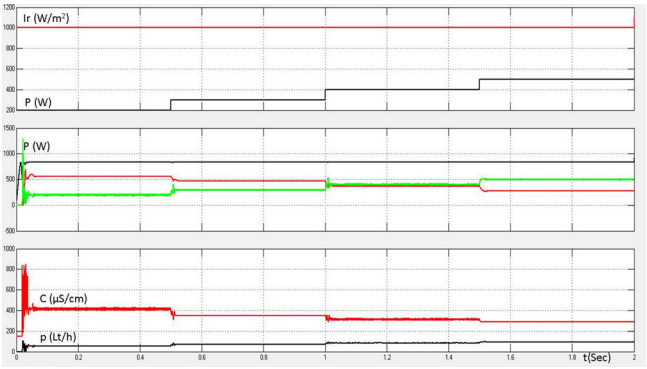

Fig. 22. (a) Solar irradiance and set point of the consumed power by the desalination plant, (b) power generated by the PV source (black), power consumed by the desalination plant (green) and power saving in the power bank (red), and (c) water electrical conductivity (red) and water flow (black).

the flow of the water is low, and the electrical conductivity is about 420 μs/cm; as the consumed power is rising, both the flow of the water and the quality of the produced water are increased (increase of water quality means reduction of electrical conductivity).

The simulation results confirm the successful development of the RO desalination process and that the three submodels are corporate harmonically together. The model can connect to power sources and regarding the amount and the quality of power outputs results about the quality and the amount of water.

4. Conclusion and future work

This paper developed an ANFIS power model for the RO desalination plant from real data gathered by an experimental pilot desalination unit installed in the Agricultural University of Athens. The objective is to develop an accurate model that can predict the amount and the quality of the potable water concerning the power consumption. The model was developed by using the ANFIS for each output, the ANFIS for the electrical conductivity of the produced water, the ANFIS for the flow of the produced water and the ANFIS of the motor current. ANFIS can be used as an alternative way of model-free approach for modeling the whole desalination process without using complex mathematical equations. In this work, it has been shown that ANFIS models achieve good performance in the modeling of a desalination plant compared with other methods such as MLR and ANNs. The evaluation indexes such as the RMS, MAE, VAF etc. highlight the good performance of the whole model. The usability of the model is demonstrated by using the model in a simple simulation as a subpart of a power system. The model-free approach proved to be very effective in modeling RO systems even when the desalination unit is operating outside of its nominal conditions. The importance of developing such a model lies on the fact that there are no other power models of RO plant according to the literature. This model is very important for simulating power applications regarding the available power with respect to the amount and the quality of the produced water. In future wok, a power model of the desalination process is going to be developed by adding more outputs like brine flow rate and brine electrical conductivity and more inputs like water temperature.

Symbols

P	—	Power of the desalination plant, W
V	—	Voltage of the desalination plant, V
c	—	Center of the Gaussian
MAE	—	Mean absolute error
RMSE	—	Root mean square error
NDEI	—	Nondimensional error index
R^2	—	Coefficient of determination
V_{pv}	—	Voltage across the equivalent circuit, V
G_r	—	Reference solar irradiance at standard test conditions, W/m²
I_{scr}	—	Short circuit current of the PV source at standard test conditions, A
T_{pv}	—	Temperature of the PV source, °C
V_{mppr}	—	Voltage of the PV source at the MPP at STC, V

N_{vocT}	—	Temperature coefficient of the open circuit voltage
C	—	Water electrical conductivity, mS/cm
P	—	Water flow, Lt/h
σ	—	Typical deviation
VAF	—	Percentile variance accounted for
NDEI	—	Nondimensional error index
P	—	Linear correlation coefficient
T_r	—	Reference temperature at standard test conditions, °C
G_{pv}	—	Solar irradiance that incidents on the PV source, W/m²
V_{ocr}	—	Voltage across the PV source at standard test conditions, V
I_{mppr}	—	Current of the PV source at the MPP at STC, A
n_{iscT}	—	Temperature coefficient of the short circuit current

References

[1] D. Libotean, J. Giralt, F. Giralt, R. Rallo, T. Wolfe, Y. Cohen, Neural network approach for modeling the performance of reverse osmosis membrane desalting, J. Membr. Sci., 326 (2009) 408–419.

[2] R. Segurado, J.F.A. Madeira, M. Costa, N. Duić, M.G. Carvalho, Optimization of a wind powered desalination and pumped hydro storage system, Appl. Energy, 177 (2016) 487–499.

[3] J.R. Werber, A. Deshmukh, M. Elimelech, Can batch or semi-batch processes save energy in reverse-osmosis desalination? Desalination, 402 (2017) 109–122.

[4] E. Dimitriou, E.S. Mohamed, C. Karavas, G. Papadakis, Experimental comparison of the performance of two reverse osmosis desalination units equipped with different energy recovery devices, Desal. Wat. Treat., 55 (2015) 3019–3026.

[5] E. Dimitriou, E.S. Mohamed, G. Kyriakarakos, G. Papadakis, Experimental investigation of the performance of a reverse osmosis desalination unit under full- and part-load operation, Desal. Wat. Treat., 53 (2014) 3170–3178.

[6] S. Sobana, R.C. Panda, Development of a transient model for the desalination of sea/brackish water through reverse osmosis, Desal. Wat. Treat., 51 (2013) 2755–2767.

[7] K.A. Al-shayji, S. Al-wadyei, A. Elkamel, Modelling and optimization of a multistage flash desalination process, Eng. Optim., 37 (2005) 591–607.

[8] M. Jafar, A. Zilouchian, Application of Soft Computing for Desalination Technology, Intelligent Control Systems Using Soft Computing Methodologies, CRC Press, Boca Raton, FL, USA, 2001.

[9] K. Zhani, H. Ben Bacha, Modeling and simulation of a new design of the SMCEC desalination unit using solar energy, Desal. Wat. Treat., 21 (2010) 346–356.

[10] D. Libotean, Modeling the Reverse Osmosis Processes Performance Using Artificial Neural Networks, PhD Dissertation, Department of Chemical Engineering, Rovira I Virgili University, Tarragona, 2007.

[11] R.W.F. He, D. Han, C. Yue, W.H. Pu, A parametric study of a humidification dehumidification (HDH) desalination system using low grade heat sources, Energy Convers. Manage., 105 (2015) 929–937.

[12] L. Perkovic, T. Novosel, T. Pukšec, B. Cosic, M. Mustafa, G. Krajacic, N. Duica, Modeling of optimal energy flows for systems with close integration of sea water desalination and renewable energy sources: case study for Jordan, Energy Convers. Manage., 110 (2016) 249–259.

[13] H.-J. Oh, T.-M. Hwang, S. Lee, A simplified simulation model of RO systems for seawater desalination, Desalination, 238 (2009) 128–139.

[14] F.N. Alasfour, H.K. Abdulrahim, Rigorous steady state modeling of MSF-BR desalination system, Desal. Wat. Treat., 1 (2009) 259–276.

[15] J.S.R. Jang, ANFIS: Adaptive-Network-Based Fuzzy Inference System, IEEE Transactions on Systems, Man, and Cybernetics, Vol. 23, 1993, pp. 665–685.

[16] J.S.R. Jang, C.-T. Sun, Neuro-Fuzzy Modeling and Control, Proc. IEEE, 83 (1995) 378–406.

[17] M. Inal, Determination of dielectric properties of insulator materials by means of ANFIS: a comparative study, J. Mater. Process. Technol., 195 (2008) 34–43.

[18] R. Singh, A. Kainthola, T.N. Singh, Estimation of elastic of rocks using an ANFIS approach, Appl. Soft Comput., 12 (2012) 40–45.

[19] A. Khajeh, H. Modarress, B. Rezaee, Application of an adaptive neuro-fuzzy inference system for solubility prediction of carbon dioxide in polymers, Expert Syst. Appl., 36 (2009) 5728–5732.

[20] A. Melit, Artificial Intelligence-Based Modeling for Sizing of a Stand-Alone Photovoltaic Power System: Proposition for a New Model Using Neuro-Fuzzy Systems (ANFIS), 3rd International IEEE Conference on Intelligence Systems, London, UK, 2006, pp. 606–611.

[21] A.I. Dounis, G. Leftheriotis, S. Stavrinidis, G. Syrrokostas, Electrochromic device modeling using an adaptive neuro-fuzzy inference system: a model-free approach, Energy Build., 110 (2016) 182–194.

[22] E.S. Mohamed, G. Papadakis, E. Mathioulakis, V. Belessiotis, A direct-coupled photovoltaic seawater reverse osmosis desalination system toward battery-based systems — a technical and economical experimental comparative study, Desalination, 221 (2008) 17–22.

[23] E.S. Mohamed, G. Papadakis, E. Mathioulakis, V. Belessiotis, An experimental comparative study of the technical and economic performance of a small reverse osmosis desalination system equipped with hydraulic energy recovery unit, Desalination, 194 (2006) 239–250.

[24] E.S. Mohamed, G. Papadakis, E. Mathioulakis, V. Belessiotis, The effect of hydraulic energy recovery in a small sea water reverse osmosis desalination system; experimental and economical evaluation, Desalination, 184 (2005) 241–246.

[25] B. Windrow, M.A. Lehr, 39 Years of Adaptive Neural Networks: Perceptron, Madiline and Backpropagation, Proc. IEEE, Vol. 78, 1990, pp. 1415–1442.

[26] H. Ying, General SISO Takagi–Sugeno fuzzy systems with linear rule consequent are universal approximators, IEEE Trans. Fuzzy Syst., 6 (1998) 582–587.

[27] T. Tagaki, M. Sugeno, Fuzzy Identification of Systems and Its Applications to Modeling and Control, IEEE Transactions on Systems, Man, and Cybernetics, Vol. 15, 1985, pp. 116–132.

[28] B. Hartmann, O. Banfer, O. Nelles, A. Sodja, L. Teslic, I. Skrjanc, Supervised hierarchical clustering in fuzzy model identification, IEEE Trans. Fuzzy Syst., 19 (2011) 1163–1176.

[29] MATLAB Manual, Fuzzy Logic Toolbox User's Guide, The MathWorks Inc., Massachusetts, USA, 2009.

[30] P. Kofinas, G. Vouros, A.I. Dounis, Energy Management in Solar Microgrid via Reinforcement Learning, Proc. 9th Hellenic Conference on Artificial Intelligence (SETN '16), Article 12, ACM, Thessaloniki, Greece, 2016, p. 7.